Acta Biomaterialia 10 (2014) 3546–3556

Contents lists available at ScienceDirect

Acta Biomaterialia

journal homepage: www.elsevier.com/locate/actabiomat

Synergistic hierarchical silicone-modified polysaccharide hybrid as a soft scaffold to control cell adhesion and proliferation

Wei-Chen Huang [a], Kun-Ho Liu [b], Ta-Chung Liu [a], Dean-Mo Liu [a], San-Yuan Chen [a,*]

[a] Department of Materials Sciences and Engineering, National Chiao Tung University, Hsinchu 30010, Taiwan
[b] Advanced Delivery Technology Co. Ltd, 5F, D Building, No. 120, Zhonghua Rd, Hsinchu Industrial Park, Hukou Township, Hsinchu 30352, Taiwan

ARTICLE INFO

Article history:
Received 17 December 2013
Received in revised form 17 April 2014
Accepted 24 April 2014
Available online 2 May 2014

Keywords:
Amphiphilic copolymer
Cell adhesion
Interface manipulation
Mechanical stiffness
Topography

ABSTRACT

In this study, a new type of polydimethylsiloxane-modified chitosan (PMSC) amphiphilic hydrogel was developed as a soft substrate to explore cellular responses for dermal reconstruction. The hydrogel wettability, mechanical stiffness and topography were controllable through manipulation of the degree of esterification (DE) between hydrophobic polydimethylsiloxane (PDMS) and hydrophilic N,O-(carboxymethyl)-chitosan (NOCC). Based on microphase separation, the incorporation of PDMS into NOCC increased the stiffness of the hybrid through the formation of self-assembled aggregates, which also provided anchor sites for cell adhesion. As the DE exceeded 0.39, the size of the PDMS-rich aggregates changed from nanoscale to microscale. Subsequently, the hierarchical architecture resulted in an increase in the tensile modulus of the hybrid gel up to fourfold, which simultaneously provided mechano-topographic guidance and allowed the cells to completely spread to form spindle shapes instead of forming a spherical morphology, as on NOCC (DE = 0). The results revealed that the incorporation of hydrophobic PDMS not only impeded acidic damage resulting from NOCC but also acted as an adhesion modification agent to facilitate long-term cell adhesion and proliferation on the soft substrate. As proved by the promotion on long-term type-I collagen production, the PMSC hybrid with self-assembled mechano-topography offers great promise as an advanced scaffold material for use in healing applications.

1. Introduction

In tissue engineering, interface manipulation plays an important role in the control of the cell transition between materials and emergent tissues [1,2]. Materials with specific topography, mechanical properties and functional groups provide both physical and chemical signals to regulate cell functions, including adhesion, spreading, migration and proliferation [3–7]. Although a number of reports have been devoted to investigating the interfacial interaction between cells and rigid substrates, there have been few studies focusing on analyzing in situ the cellular response to soft polymeric substrates, which are thought to be crucial for providing the substrate with stability for long-term restoration [6,7].

Hydrogel-based materials have been demonstrated to be the most attractive biomaterials due to the structural similarity to the natural extracellular matrix, and can be further developed as soft substrates because of the absorption capacity, moisture retainability and permeability to nutrients [1–5,8,9]. However, due to the solvation and the dissociation effects, the polymer chains in the cellular aqueous environment tend to cause the formation of a hydrated interface, pH deviance and structural rearrangement. Such inevitable phenomena will inhibit the cell–matrix adhesions. Thus, the main challenge lies in adjusting the material essential features to determine the optimal physical and chemical conditions required for cell–matrix adhesions. Herein, we have designed a new type of covalent amphiphilic polymer network (CAPN) formed by chemical cross-linking with hydrophilic and hydrophobic polymer segments to explore the cell–substrate interaction on the soft substrates.

As is well known, chitosan-based hydrogel has been largely developed in biomedical applications such as tissue engineering, gene/drug delivery and wound healing due to the distinct structural similarities to the mammalian glycosaminoglycans (GAGs) [36–41]. By improving the limited solubility and water-retention ability of chitosan, the natural polymer N,O-(carboxymethyl)-chitosan (NOCC) has been developed in our laboratory and has shown excellent characteristics, including antimicrobial activity, water-retention abilities and the promotion of fibroblast proliferation [11,12]. However, if used as a soft substrate for cell adhesion and proliferation, the poor mechanical properties and acidic damage associated with the hydrophilic nature of NOCC will become

* Corresponding author.
E-mail address: sanyuanchen@mail.nctu.edu.tw (S.-Y. Chen).

http://dx.doi.org/10.1016/j.actbio.2014.04.025
1742-7061/

barriers difficult to overcome. In contrast, polydimethylsiloxane (PDMS), an elastic and non-polar polysiloxane, is well-known as an artificial adhesive that is environmentally inert enough to provide a strongly protective, biocompatible and self-adherent environment for surrounding tissues [13]. By taking advantage of the esterification reaction between bis(hydroxyalkyl) terminated polydimethylsiloxane (PDMS diol, also known as silicone) and NOCC, a new type of hierarchically structured hybrid hydrogel, called PDMS–NOCC amphiphilic polymer network (PMSC), was formed. The hydrogel displays a synergetic effect combined with the merits of both NOCC and PDMS. On the one hand, the hydrophilic NOCC offered excellent water-retention and absorption ability; on the other hand, the hydrophobic PDMS imparted the improvement on structural and mechanical properties through forming the co-continuous but immiscible units of networks by microphase separation [14,15]. In such an amphiphilic hydrogel system, the hydration of the hydrophilic–hydrophobic polymeric hybrid is supposed to considerably influence the affinity of cells because the interfacial energy is altered with the change in the bound water between networks, which in turn directly interferes with cell attachment [10]. The specific mechanical and topographic cues of the self-assembling hierarchical architecture also critically affect the cell response, especially the long-term behaviors and restoration. Therefore, the exploration is very important for understanding how the environmental cues of amphiphilic networks with different degrees of hydrophilicity/hydrophobicity can chemically and physically impact on the cell adhesions.

In addition, to fabricate a soft substrate for better control over cell function, it is usually necessary to mimic the ECM microenvironment with the inclusion of adhesion reagents such as collagen, RGB and fibronectin. However, these adhesion reagents may deteriorate due to their limited environmental adaptability to changes in pH and temperature or mechanical attack [16,17]. In this study, the hydrophobic and flexible PDMS segments in the PMSC hybrids could self-assemble into stiff aggregates as localized adhesive motifs to mechanically and topographically induce cell adhesions. When cells sense the stiffness of these PDMS-rich aggregations, the focal adhesions (FAs) composed of numerous proteins can be generated to exert internal forces and transmit signals to stimulate cellular behaviors on the PMSC hybrids [42]. Thus, these structure-enhanced hybrids that favor cell–cell communication were recognized as efficient substrates for cell growth, particularly for long-term cellular responses including cell adhesion, cell spreading, cell proliferation, alteration of cell morphology and ECM production. Through the precise manipulation of the chemical, physical and biological properties of PMSC, a new soft substrate can be developed for potential applications toward dermal reconstruction.

2. Materials and methods

2.1. Materials

Chitosan (MW = 260,000 g mol^{-1}, deacetylation degree = 80%, insoluble impurity k < 1%), 2-propanol, sodium hydroxide, chloroacetic acid, bis(hydroxyalkyl) terminated polydimethylsiloxane (PDMS diol, Mw = 5600 g mol^{-1}), 3-(4,5-dimethylthiazol-2-yl)-2,5-diphenyltetrazolium bromide (MTT), 2-(4-iodophenyl)-3-(4-nitrophenyl)-5-(2,4-disulfophenyl)-2H-tetrazolium (WST-1), phosphate-buffered saline (PBS), low glucose Dulbecco's modified Eagle's medium (DMEM) and fetal bovine serum (FBS) were purchased from Sigma–Aldrich and used as-received without further purification. The actin cytoskeleton and focal adhesion staining kit (Cat No. FAK100) was obtained from Millipore. The Sircol™ collagen assay kit was purchased from Biocolor Ltd.

2.2. Preparation of PMSC amphiphilic hydrogel

As described in our previous report, the PMSC copolymer was prepared by a two-step synthesis: carboxymethylation and esterification [18]. Briefly, the first step was the synthesis of NOCC that was performed by grafting carboxymethyl groups onto the amino site (N-site) and the hydroxyl site (O-site) of the pristine chitosan. First, 5 g of chitosan was suspended in 2-propanol (50 ml) at room temperature while being stirred for 30 min. The resulting suspension was gently mixed with 12.5 ml NaOH solution. The mixture containing NaOH (13.3 N) was mixed with 25 g of chloroacetic acid to prepare a carboxymethyl chitosan. For esterification, 2 g of dried NOCC sample was dissolved in distilled water (50 ml) and stirred for 24 h. The resulting solutions were mixed with methanol (50 ml) and stirred vigorously for 4 h. Bis(hydroxyalkyl) terminated PDMS was added at a PDMS:NOCC molar ratio of 0, 5:1, 10:1, 25:1, 50:1 and 100:l. After catalysis with sulfuric acid, the mixture was maintained and reacted at 60 °C for 24 h for esterification. After repeating the 24 h dialysis with ethanol/diethyl ether (9:1 (v/v)) three times, the purified product was obtained through drying at 50 °C overnight.

2.3. Characterization of the PMSC hybrid hydrogels

Nuclear magnetic resonance (NMR) was used to characterize PMSC. Proton NMR was performed on a 500 MHz Varian Unity Inova NMR spectrometer. The chemical structure of PMSC, NOCC and PDMS was revealed using D_2O (for PMSC and NOCC) and deuterated chloroform ($CDCl_3$, for PDMS) as solvents. The chemical shift at 1.9 ppm was taken as the reference to normalize the calculation of integration areas. The chemical shifts at 3.9 and 4.2 ppm were assigned to the protons of O$\mathbf{C}$H$_2$COOH (O-position) and N$\mathbf{C}$H$_2$COOH (N-position) of NOCC, respectively. However, after esterification happened between –COOH of NOCC and –OH of PDMS, the area of chemical shifts at 3.9 and 4.2 ppm would be reduced, and the amount was represented by $(\mathrm{Area}_{3.9ppm} + \mathrm{Area}_{4.2ppm})_{NOCC} - (\mathrm{Area}_{3.9ppm} + \mathrm{Area}_{4.2ppm})_{PMSC}$. Therefore, we defined the degree of esterification (DE) as the ratio of the consumed amount of –COOH groups $((\mathrm{Area}_{3.9ppm} + \mathrm{Area}_{4.2ppm})_{NOCC} - (\mathrm{Area}_{3.9ppm} + \mathrm{Area}_{4.2ppm})_{PMSC})$ to the original ones $((\mathrm{Area}_{3.9ppm} + \mathrm{Area}_{4.2ppm})_{NOCC})$, which can be represented by the following equation [15]:

$$DE = \frac{(\mathrm{Area}_{3.9ppm} + \mathrm{Area}_{4.2ppm})_{NOCC} - (\mathrm{Area}_{3.9ppm} + \mathrm{Area}_{4.2ppm})_{PMSC}}{(\mathrm{Area}_{3.9ppm} + \mathrm{Area}_{4.2ppm})_{NOCC}} \quad (1)$$

The PMSC hybrid hydrogels were prepared by casting a 1 wt.% water solution of 10 g onto a dish with a diameter of 3 cm with dehydration at 50 °C for 1 day. Fluorescence-labeled hydrogels which were obtained by coupling the hydrogels with fluorescein isothiocyanate (FITC) were examined by confocal microscopy (Axiovert 100 M). The composition of PMSC hydrogels in the hierarchical structure was determined by scanning electron microscopy (SEM) with energy-dispersive X-ray spectroscopy (EDX) mapping (JEOL 6700, Japan) at an acceleration voltage of 5 kV. The wetting ability was examined using the water contact angle with a VCA Optima contact angle (CA) analyzer. To examine the surface topology, 1 wt.% dispersions were fabricated into ultra-thin hydrogels on a glass slide. Atomic force microscopy (AFM) analysis was performed with the Bruker Innova atomic force microscope in tapping mode using Tap300 cantilevers. The scan rate was 0.4 Hz, and the scanning dimensions were set to 50 × 50 μm^2 for NOCC and PMSC (DE = 0.39), and 100 × 100 μm^2 for PMSC (DE = 0.61). In the force–deflection mode of AFM, the contact mode is applied to set the z-ramping with the tip at a single XY probe position on PMSC with DE = 0.39, which was scanned in advance to obtain

the topographic and phase images [19]. Strain–stress measurement was performed on the prepared hydrogels with a commercial test machine (MTS Tytron 250). Each dry sample was cut into a dog-bone shape that was 3 cm long and 1 cm wide. The sample was swollen to achieve equilibrium water content in a steam bath with the same closed system using PBS for 48 h. With a working rate of 0.1 mm s^{-1}, the tensile modulus was represented and obtained from the slope of the linear part of the strain–stress profiles.

2.4. Cell culture

Human HS68 fibroblasts obtained from the Food Industry Research and Development Institute (Hsinchu, Taiwan) were cultured in DMEM with 10% FBS, 100 μg ml^{-1} penicillin and 100 μU ml^{-1} streptomycin and were maintained in a 5% CO_2 humidified atmosphere at 37 °C.

2.5. Observation and quantification of adhered cells

For the cell adhesion assay, hydrogels were casted on 24-well plates and then were UV sterilized before the cell-culture study. Four repeated experiments were performed for each sample at each time point. The cells were trypsinized and suspended in fresh complete DMEM, and 2 ml of the cell suspension containing 4×10^4 cells was seeded in each well to achieve a solute content of 2 mg ml^{-1} in the medium. The plate was then left undisturbed at 37 °C in 5% CO_2 for 1, 2, 6, 12, 24 or 48 h. The fibroblasts on the hydrogels were stained with calcein AM for 40 min, followed by observation using confocal microscopy (Axiovert 100 M) with the fluorescence emission at 530 nm.

2.6. In situ investigation of adhered cells

To investigate the activity of the adhered cells, the WST-1 assay was performed to evaluate the mitochondrial activity. The medium composed of complete DMEM without phenol red was directly added with 10% WST-1 solution at each time point of cell adhesion (1, 2, 6, 12, 24 and 48 h). After 4 h incubation, the medium was removed and centrifuged to remove the cell debris before measurement. The cell activity of the purified medium (200 μl), which was represented by the absorbance at 450 nm, was measured using a microplate reader (TECAN Sunrise, Switzerland). In addition, the appearance of the adhered cells was observed by staining with calcein AM and demonstrated the live cells as green fluorescence.

2.7. Quantification of cell morphology

To quantify the cell shape and area, the shape index (SI), which is used to define the roundness of a cell, was determined by image analysis. With the incorporation of the observed cell area and cell perimeter, SI values were obtained using the following equation [20]:

$$\text{Shape index} = 4\pi\left(\frac{\text{cell area}}{(\text{cell perimeter})^2}\right), \quad (2)$$

where an SI value of 1 indicates a spherical cell and an SI value of 0 represents a spindle-shaped cell that is almost line-shaped. The cell area and cell perimeter were characterized for each sample after 48 h of adhesion. The calculations were performed for at least 10 different cells from each sample in at least five areas ($n > 3$).

2.8. Immunostaining

HS68 cells were cultured on coverslips coated with NOCC and PMSC hybrids at a solid content of 2 mg ml^{-1} with 2 ml medium. After incubation and two PBS washes, HS68 cells were fixed with 3.7% formaldehyde. Permeabilization was performed with 0.1% Triton X-100 for another 15 min. After three PBS washes, immunofluorescence staining with TRITC-conjugated phalloidin was performed for 2 h, and 4′,6-diamidino-2-phenylindole (DAPI) staining was performed for another 1 h. The number of adhered cells was determined via counting the number of stained nuclei using fluorescence microscopy (20× objective lens) in 10 different fields [3]. To visualize focal adhesions, vinculin staining was also performed by incubation with a monoclonal anti-vinculin antibody at 4 °C overnight, followed by incubation with a FITC-antimouse immunoglobulin G secondary antibody at room temperature for another 1 h. Finally, coverslips were mounted on fresh glass slides with mounting solution (Dako). Two- and three-dimensional cell adhesion was observed by fluorescence confocal microscopy using a Nikon C1 plus confocal system.

2.9. Collagen production

The amount of collagen was estimated using a Sircol collagen assay kit according to the manufacturer's instructions. Briefly, after cell culture in DMEM with 2.0 mg ml^{-1} sample suspensions for 5 days, 1 ml of cell culture medium was extracted from each sample and incubated with 200 μl of isolation & concentration reagent overnight at 4 °C. After centrifugation to remove the supernatant, the dye reagent was added and the sample was agitated for 45 min. Then, the SR dye was released from the collagen pellet with an alkali reagent. Spectrophotometric readings were taken in a microplate reader (TECAN Sunrise, Switzerland) at 540 nm. The test was performed three times with and without 10% FBS.

2.10. Statistical analysis

All the data were reported as means ± standard deviations (SDs) of the similar studies performed in triplicate. Statistical analysis was carried out by one-way analysis of variance (ANOVA) followed by Tukey's post hoc test for statistical analysis to determine statistical significance ($p < 0.05$).

3. Results and discussion

3.1. Structural and rheological properties of PMSC hybrids

PMSC with hierarchical structure was synthesized using the esterification reaction between the carboxylic groups of NOCC and the hydroxyl groups of PDMS, as shown in Fig. 1a. The super-porous aggregates are indicated as cross-linked points between the nearby heterogeneous networks (shown in the red frame in Fig. 1a). Scheme 1 illustrates the self-assembling procedure of the PMSC CAPNs. The hydrophilic and hydrophobic segments of PMSC underwent morphological isomerization via the solvation effect of water. After water elimination, the rising salt ion effect between the abundant $-COO^-$ and $-NH_3^+$ groups resulted in the formation of a dense, hierarchical structure [15]. Upon swelling, the microarchitecture developed into aggregates with super-porous structures dispersed in the matrix, leading to the enhancement of water absorbability. EDX mapping of the SEM image demonstrated that the elements Si and C were prevalent in the aggregates of the PMSC hybrid, providing evidence that the aggregates were mainly composed of PDMS (Fig. 1b). Therefore, the Si element content and the DE obtained from XPS analysis and

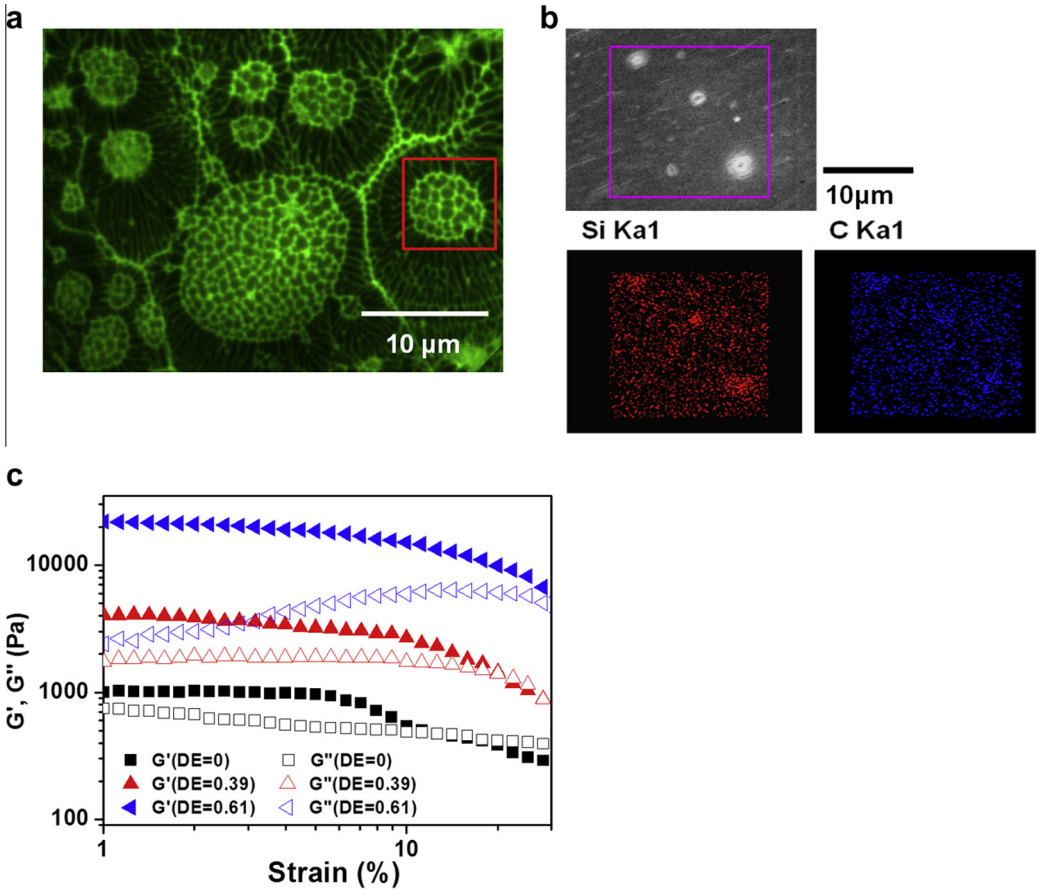

Fig. 1. (a) Fluorescent microscopic image of PMSC (DE = 0.61) conjugated with FITC to illustrate the swollen spherical-porous macrostructures (inside the red square) with polygonal architecture. (b) SEM image and EDX mapping of the PMSC to present the distribution of elements Si and C. (c) Rheological properties of NOCC (DE = 0), PMSC (DE = 0.39) and PMSC (DE = 0.61) hydrogels.

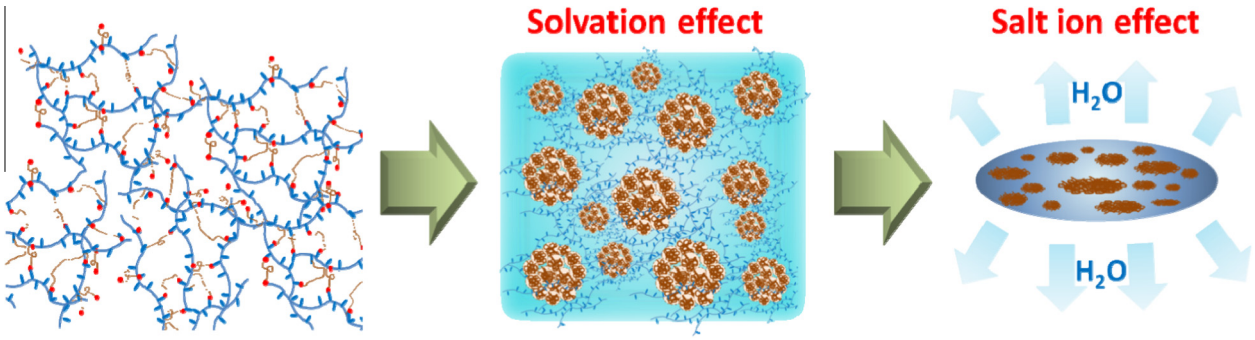

Scheme 1. Schematic representation for the self-assembling procedure of PMSC CAPNs. First, the solvation effect from water caused the morphological isomerization of the hydrophilic and hydrophobic segments of PMSC. This was followed by the thermally induced water elimination; the salt ion effect rising between the abundant $-COO^-$ and $-NH_3^+$ groups contributed to the formation of a dense and hierarchical structure.

NMR analysis, respectively, could be considered as the aggregation density of the PMSC hybrids, as shown in Table 1. It was found that the ultimate value of the aggregation density was controlled to be 0.61 at a molar ratio of PDMS:NOCC = 100:l.

The rheological properties of NOCC and PMSC (with DE = 0.39 and DE = 0.61) hydrogels were obtained by strain sweep tests on the hydrated samples to monitor the storage modulus (G') and loss modulus (G''). As shown in Fig. 1c, all samples underwent a breakdown of the gel state to a quasi-liquid state at the threshold strain γ_c, which was defined as a gel–liquid transition point when $\tan\delta = G'/G'' = 1$ [43]. The γ_c value is 12.4%, 20.6% and 35.5% for NOCC (DE = 0), PMSC (DE = 0.39) and PMSC (DE = 0.61),

Table 1
Characterization on the synthesis of hierarchical PMSC based on the degree of esterification by NMR and element concentration by XPS.

Sample ID	Molar ratio PDMS:NOCC	NMR analysis	Element composition by XPS analysis		
		DE value	C1*s* (%)	O1*s* (%)	Si2*p* (%)
NOCC	0	0	43.8	56.2	0
PMSC	5:1	0.15	30.6	66.2	3.2
	10:1	0.26	27.3	64.9	7.8
	25:1	0.39	27.5	60.5	12.0
	50:1	0.51	29.9	53.4	16.7
	100:1	0.61	36.5	44.0	19.5

respectively, indicating that the hydrogel with higher DE displayed a larger strain before being deformed, which can be attributed to the incorporation of PDMS to strengthen the network structure. In addition, it can be found that with the increase of DE, both the G' and G'' modulus increased. Based on the rubber elasticity theory, the storage modulus is correlated to the network cross-link density represented as $G = gRTN$, where G is the network equilibrium shear modulus, g is a constant close to 1.0 for incompressible materials, R is the gas constant, T is the absolute temperature and N is the number of elastically active network chains per unit volume [44]. For PMSC hydrogels, the self-assembled PDMS-rich aggregations with a higher DE value enhanced the network structure due to the higher N value, which resulted in the increase in both values of G' and G''.

3.2. Adhesion of human dermal fibroblasts on the PMSC hybrid

The number of cells adhering to the PMSC hybrids was determined after 2 and 48 h of incubation, as demonstrated in Fig. 2a. After 2 h of incubation, the number of adherent cells decreased as the DE increased. The cell density on the NOCC was estimated to be 7251 cells cm^{-2}, while the PMSC hybrid with the largest DE value of 0.61 had the lowest cell density of 1600 cells cm^{-2}. However, after 48 h of incubation, the attached cell density of NOCC decreased to 2520 cells cm^{-2}. In contrast, the PMSC hybrid exhibited the highest adherent cell density of 7592 cells cm^{-2}. As shown in the fluorescent microscopy images of Fig. 2b, the adhered cells on NOCC displayed spherical cell morphology after 48 h, which suggested a difficult connection to nearby cells due to the loss of filopodia. For the PMSC hybrid with a DE of 0.39, the cell adhesion density was obviously increased compared to that of NOCC. However, on the PMSC hybrid with a DE of 0.61, the morphology of the adhered cells changed from spherical to spindle-shape after 48 h adhesion. It implied that cells with extensive filopodia were capable of growth, migration and proliferation. Such morphogenesis indicated that HS68 fibroblasts were able to efficiently grow on the PMSC hybrids without modification by adhesion proteins such as RGB, fibronectin and collagen.

3.3. Short-term attachment/adhesion of HS68 fibroblasts on PMSC hybrids

The compatibility of a cellular system with respect to a substrate can be evaluated after 2 and 48 h of adhesion, which represents the short-term cell attachment and long-term cell spreading/growth/proliferation, respectively [21]. After 2 h of cell adhesion, we found that the ratio of attached cells decreased from 23% to 6% as the DE increased from 0 to 0.61 (Fig. 3a). In the short-term attachment/adhesion period, cell behavior was consistent with the DLVO theory, in which there is competition between

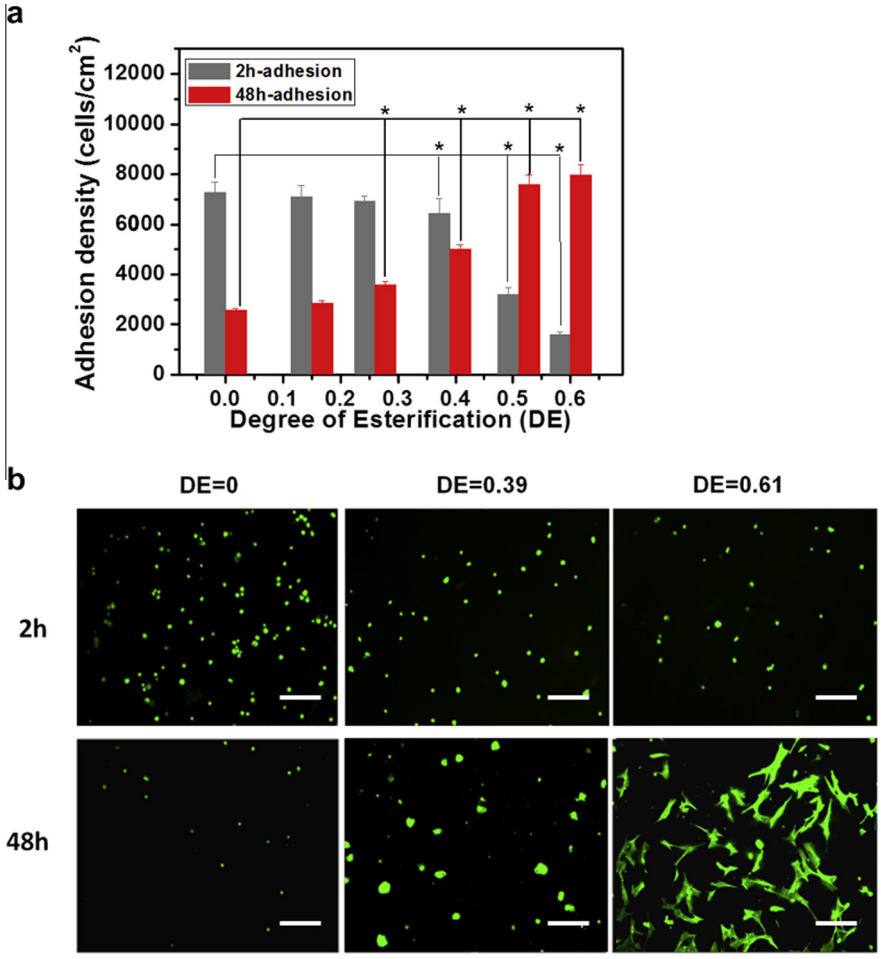

Fig. 2. (a) Cell counting after 2 and 48 h adhesion demonstrated that the adhered cells decreased with the increase of DE for short-term adhesion, while there was an opposite tendency for the long-term adhesion. $^{*}p < 0.05$ when compared with NOCC groups (DE = 0). (b) Fluorescent microscopic images (10× objective) demonstrating the different cell distribution and morphology of human dermal fibroblasts (HS68) between PMSC with DE = 0, 0.39 and 0.61 after 2 and 48 h adhesion stained by calcein AM live stain (scale bar equals 200 μm on all the images).

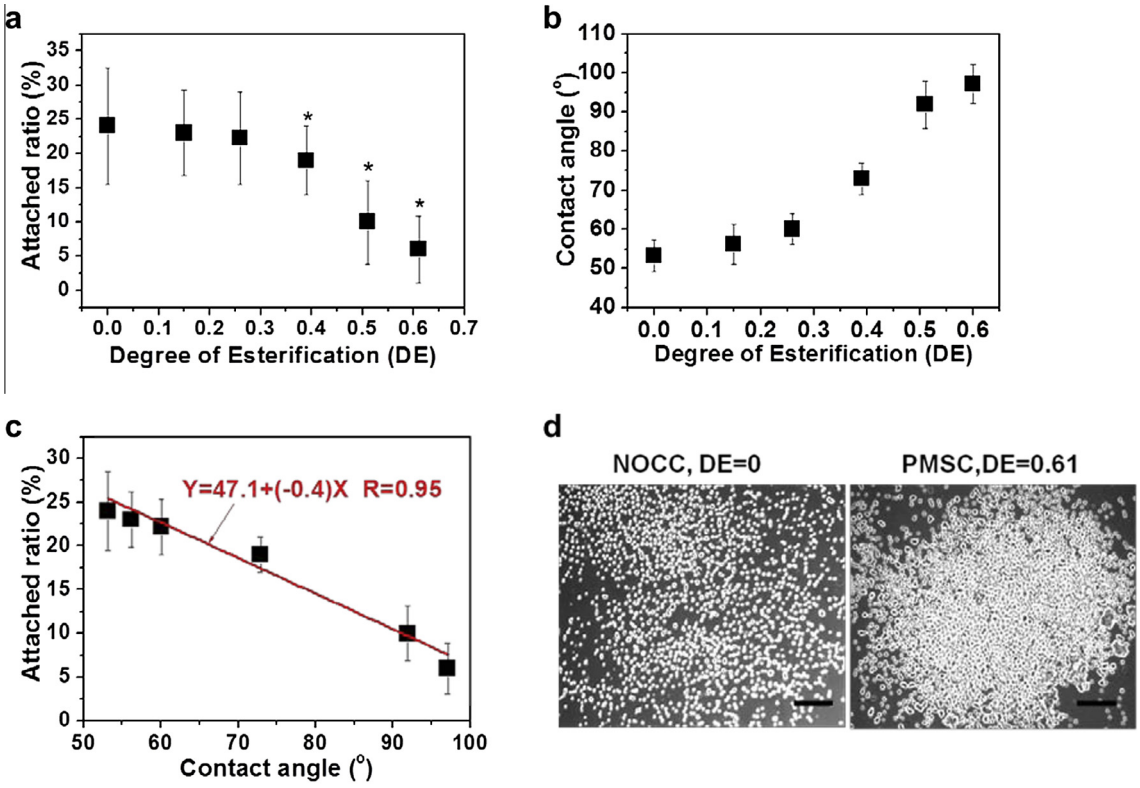

Fig. 3. (a) The PMSC substrate with higher DE presenting the lower cell adhesion ratio by 2 h attachment. $^{*}p < 0.05$ when compared with NOCC groups (DE = 0). (b) CA measurement, indicating that the surface was changed from being hydrophilic to hydrophobic with increasing DE. (c) A linear relationship between CA of the PMSC hybrid and the ratio of attached cell, obtained via linear fitting. (d) Optical microscopic images (10× objective) showing the cell distribution on NOCC and PMSC after 2 h incubation (scale bar equals 200 μm on the image).

cell-to-cell cohesiveness and cell-to-substrate adhesivity, which is determined by the surface free energy of the used substrate [22–24]. Generally, cells have more potential to become wetted on surfaces with higher surface free energy because the hydrophilic groups tend to immobilize the adhesion proteins inside the hydration layer [23,25]. To further investigate the interaction between cells and substrates, the contact angle (CA) representing the wetting ability was analyzed. As shown in Fig. 3b, we found that the CA of the PMSC hybrid increased from 53° to 97° as the DE was increased from 0 to 0.61. Particularly, when the DE was less than 0.39, the surface of the hybrid exhibited hydrophilicity (CA < 90°). When the DE exceeded 0.51, a CA larger than 90° indicated that the surface became hydrophobic. Furthermore, a linear relationship between the CA of the hybrid and the ratio of the attached cells can be observed in Fig. 3c and given as:

$$Y = -0.41X + 47, \tag{3}$$

where X is the CA value in the range from 53° to 97° and Y is the corresponding ratio of cells that are attached to the hybrids.

The results strongly indicate that PDMS incorporation influenced the surface wettability. Specifically, the hydrophobicity of the surface increased with the replacement of the non-polar polysiloxane chains on –COOH, which further inhibited cell attachment. Hence, the DE value was thought to be a dominant factor in controlling short-term cell adhesion. As demonstrated in Fig. 3d through in situ monitoring by optical microscopy, cell–cell aggregates on the underlying PMSC with a DE > 0.39 were more distinct than those on NOCC, indicating that the cell wettability was weaker on PMSC after short-term cell culture.

3.4. Long-term spreading/proliferation of HS68 fibroblasts on PMSC hybrids

To observe cell activity on NOCC and PMSC at various time points, including 0, 2, 6, 12, 24 and 48 h, a WST-1 assay was used to monitor the real time activity of both the adhered and suspended cells. The assay was chosen because it is a more sensitive method than cell counting. With the absorbance at $\lambda = 450$ nm, the activity of cells incubated with NOCC increased at the beginning of incubation, achieving a maximum absorption strength of 0.63 at 6 h, but decreased to 0.52 after 48 h. However, for the PMSC hybrid with a DE of 0.39, cell activity exhibited continuous growth with increasing incubation time (Fig. 4a). As shown by FTIR analysis (Supplementary Fig. S.1), a relatively stronger characteristic absorption of the carboxylic group (1724 cm^{-1}) appeared on the spectrum of NOCC. It indicates that the dissociation that occurred upon hydration of NOCC directly affects the pH value of the medium. As shown in Fig. 4b, the pH value of the medium with PMSC at DE = 0.39 was maintained in the range of 7.2–7.4, which is the optimal microenvironment for the growth of human fibroblasts [26]. In contrast, NOCC caused a relative reduction in the environmental pH (<7) that was far from an ideal value at all of the time points, which was attributed to the large number of hydrophilic –COOH groups on NOCC [27]. Furthermore, the extracellular pH changes toward the acidic range may considerably inhibit the synthesis of cellular matrix components [28].

A striking difference in the morphological evolution of cells after 48 h of adhesion was found, as shown in the fluorescent images of Fig. 5a. Cells that adhered to NOCC were spherical in shape with the absence of stress fibers, indicating poor spreading on the hybrid. In the case of the PMSC hybrid with a DE of 0.39,

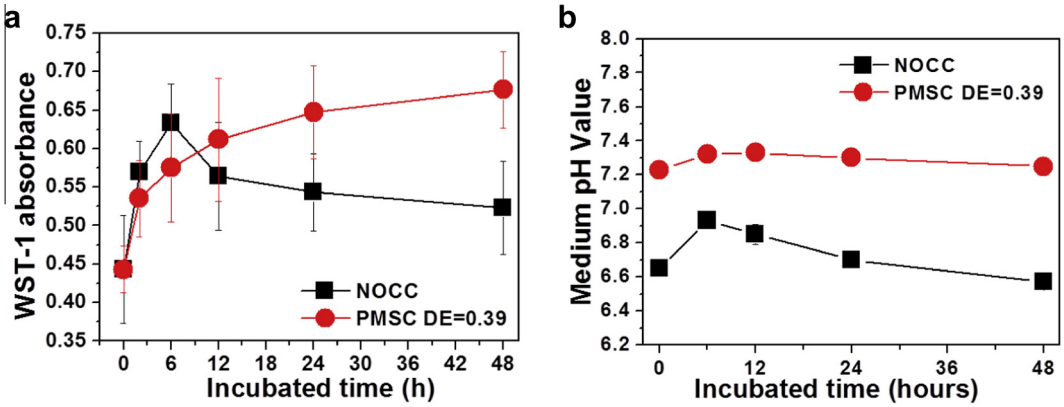

Fig. 4. (a) Cell activity on NOCC and PMSC with DE = 0.39 by 0, 2, 6, 12, 24 and 48 h was measured by WST-1 assay with absorbance at λ = 450 nm. (b) The environmental pH value changing with incubation time for cells cultured in the medium of NOCC and PMSC with DE = 0.39.

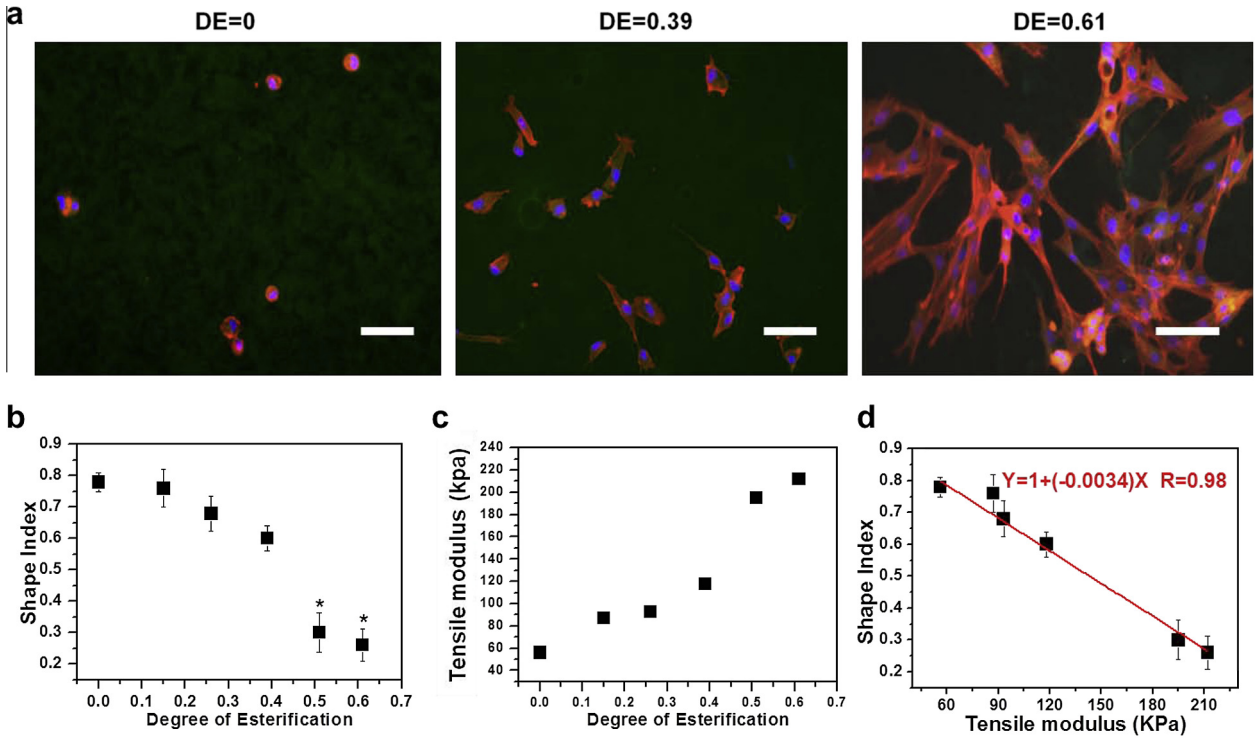

Fig. 5. (a) Representative fluorescence microscopy images (20× magnification) demonstrated the distribution and morphology of HS68 fibroblasts cultured on PMSC with DE = 0, 0.39 and 0.61 (scale bar equals 100 μm on all the images). (b) The statistical analysis of the adhered cell SI on the PMSC hybrids with different DE after 48 h adhesion. $^{*}p < 0.05$ when compared with NOCC groups (DE = 0). (c) The tensile modulus obtained by strain–stress measurement on PMSC hybrids increased with DE. (d) A linear function between the shape index and the tensile modulus of PMSC hybrids with different DE.

the adhered cells exhibited a slightly extended fibroblastic morphology with a spindle shape. As the DE of the PMSC hybrid became larger than 0.39, the adhered cells formed a confluent cluster with extended bodies that connected to neighboring companies. Because the change in cell shape through reorganization of cytoskeletal networks has been shown to be an important regulator of cell activity, statistical analysis of the SI of adhered cells on the PMSC hybrids with different DE values after 48 h adhesion was performed (Fig. 5b). For NOCC, the SI was 0.78, indicating that the cells failed to spatially reorganize on the surface [20]. With the increase in the DE to 0.39, the SI gradually decreased, and a rapid decrease in the shape index occurred below 0.3 as the DE became larger than 0.39. This implied that when the DE exceeded 0.39, the microenvironment constructed by the hybrids was adjusted to fit the cell microarchitecture, causing a significant improvement on cell spreading. To the best of our knowledge, cells reside in their native microenvironment (i.e., extracellular matrix), which provides a specific mechanical stiffness, as do most biophysical cues that direct cell morphogenesis toward hierarchically organized tissue structures [29]. Based on the strain–stress measurement shown in Fig. 5c, the tensile modulus of the PMSC hybrids rapidly increased from 118 kPa to 195 kPa as the DE exceeded 0.39, indicating that PDMS incorporation imparted a higher force for the substrate to overcome fracture. Such mechanical enhancement stimulated the cell to apply the internal force for body contraction, which deeply influenced the cell morphology and physiology, including migration and proliferation [30]. Indeed, a linear function between the shape index and the tensile modulus of PMSC

hybrids with different DE values occurred according to the following equation and as shown in Fig. 5d:

$$Y = (-0.0034)X + 1, \quad (4)$$

where X is the tensile modulus and Y is the shape index in the range $0 < Y < 0.8$.

The results demonstrated that PSMC hybrids with DE values larger than 0.39 led to a high stiffness (>195 kPa) that was sufficient to force HS68 cells to extend their stress fibers for ongoing growth.

3.5. Mechanism of adherence/spreading/proliferation of HS68 fibroblasts on PMSC hybrids

Surface analysis by AFM showed that NOCC had a smooth surface with a root-mean-square average roughness (rms, Rq) of 0.167 μm (Fig. 6a). As the DE exceeded 0.39, there were numerous protrusions or PDMS-rich aggregates (as shown in Fig. 1b) on the hybrid surface. By positioning the single probe on the phase image, the obtained deflection–displacement curve (f–d curve) as shown in Fig. 6b revealed that (1) PDMS-rich aggregates were stiffer than the surrounding networks because the slope of the approaching curve (black) obtained from the protrusions was sharper ($slope_{black} = 22.9 > slope_{red} = 18.6$) and (2) the PDMS-rich aggregates were more adhesive than the surrounding networks due to a higher pull-off deflection for the retraction [31]. As reported by Georges et al., the cellular response to substrate stiffness can be expressed by Hooke's law, $F = -Kx$, and a higher K value corresponds to a higher stiffness value, which facilitates cell traction without energy consumption [32]. In our case, the PDMS-rich aggregates played important roles as springs with a stiffness that dominated the cell morphology. As shown in Scheme 2a, a cell on a soft and smooth surface will become round in shape due to the loss of supporting forces. For topological surfaces with nanoscale PDMS-rich aggregates, the ultra-small springs are still unable to provide enough force to support a cell, so its body remained rounded (Scheme 2b). Only when cells are provided with enough mechanical force by large-scale aggregations, such as microscale springs, can they spread efficiently by applying internal forces to extend around their periphery (Scheme 2c).

In accordance with these findings, the roughness profile as shown in Fig. 6c demonstrates that a sharp transition from 0.56 nm to 1.34 nm occurred as the DE increased from 0.39 to 0.51. Accordingly, the PMSC hybrids with a DE below 0.39 exhibited a nanoscale roughness but had a microscale roughness as the DE became larger than 0.51 nm. Such large-scale PDMS-rich aggregates provided a larger stiff area that was supposed to be efficient for cell adhesion. Indeed, the observation of cell morphology (Fig. 7a) showed that the cell adhering on NOCC exhibited a spherical entity with less contact with the matrix. The SEM image further showed that the substrate was anchored with very few filopodia, which resulted in poor attachment of the main body with a sub-cellular sphere of ~10 μm in diameter. For the PMSC hybrids with a DE of 0.39, the cells spread, and the extensive skeleton was clearly visible on the confocal laser scanning microscopic (CLSM) image. However, an increase in the cell body size of ~20 μm was still predominant because the substrate was inadequate to hold cell filopodia with sufficient force. For PMSC with DE > 0.51, the whole cell body was found to spread along the substrate with clear linear arrays of actin bundles. Under these conditions, the cell tightly bonded to the substrate with the most flat and extended

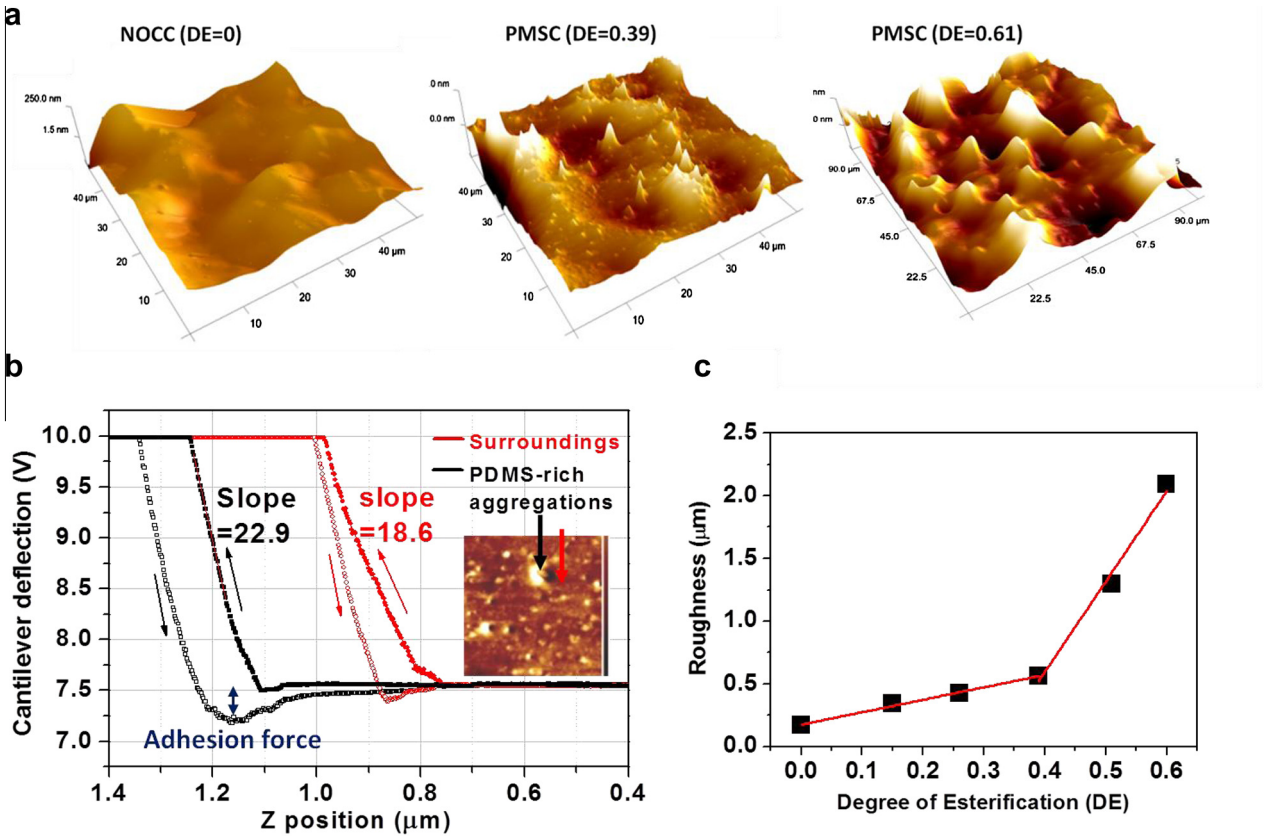

Fig. 6. (a) Topographical view of NOCC, PMSC with DE = 0.39 and DE = 0.61 obtained by AFM analysis. (b) Typical approach and retract curve based on the phase image of PMSC, demonstrating the difference in mechanical properties within the hierarchical structure of PMSC. Different regions are marked: the black curve indicates a deflection–distance curve on the as-marked PDMS-rich protrusions, and the red curve gives the indication on the surroundings. (c) The root-mean-square average roughness (rms, Rq) obtained on PMSC hybrids demonstrated an increase with the increase of DE.

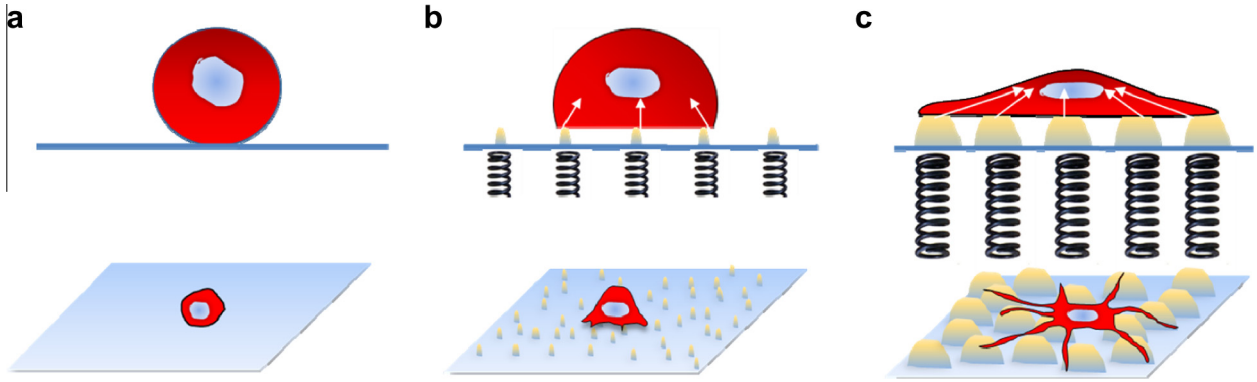

Scheme 2. The PDMS-rich aggregates played important roles as springs with adjustable stiffness to dominate cellular response. (a) A cell lying on a soft and smooth surface displays a rounded shape due to the loss of supporting forces. (b) The nanoscaled PDMS-rich aggregations are like ultra-small springs, and are still unable to support the cell so its body remained rounded. (c) The larger-scaled aggregations, like microscaled springs, can provide enough mechanical force for the cell spreading.

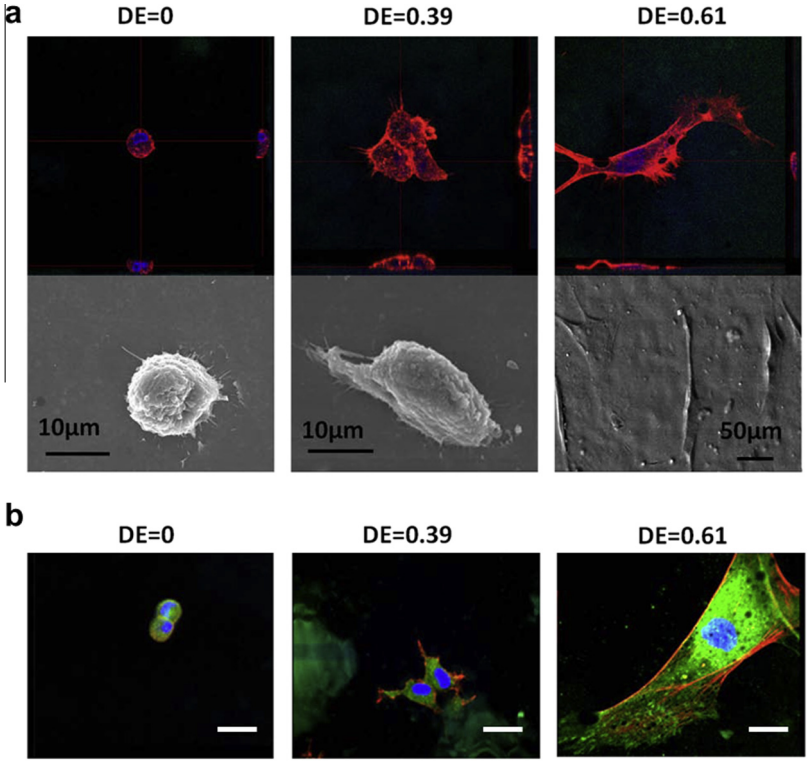

Fig. 7. (a) CLSM image (100× magnification) and representative SEM images of HS68 cells grown on the NOCC, PMSC with DE = 0.39 and DE = 0.61. A plan view and side view through the XZ and YZ showing the morphology, shape and height of cells. The cytoskeleton and nuclei were stained with TRITC-conjugated phalloidin (red) and DAPI (blue), respectively, while the as-prepared hybrids were conjugated with FITC dye. (b) Representative fluorescence microscopy images (100× magnification) of HS68s grown on NOCC, PMSC-1, PMSC-2 and PMSC-3 with immunofluorescent staining of cytoskeleton (red), nucleus (blue) and vinculin (green) after 48 h incubation (scale bar equals 20 μm on all the images).

body of more than 100 μm in body length. Through staining of vinculin, a membrane cytoskeleton protein involved in the linkage of integrin adhesion molecules, the focal adhesion was absent on the hybrids with a DE < 0.39, but the complex could be clearly visualized around the cell periphery on PMSC with a DE > 0.51 as shown in Fig. 7b [33]. In addition, the microscale PDMS-rich aggregates were slightly visible in the boundaries of the cell body. Cells tended to align along the perimeter of PDMS-rich aggregates. The results showed that only PDMS-rich aggregation in the micron-size topology efficiently provided optimal force to support and maintain cell adhesion. In other words, in spite of the effect of the hydrophobicity of PDMS on short-term cell attachment, the higher stiffness of PMSC-rich aggregates provided topographic guidance that induced strong adhesion and wild spreading of the cells.

To mimic the ECM environment, adhesion proteins such as RGB, laminin, fibronectin and collagen were generally employed to induce cell–matrix adhesions. However, these adhesion proteins not only are easily degraded but also their orientation and availability cannot be controlled. In contrast, the experimental results support the assertion that the PMSC-rich aggregates can form localized adhesive motifs to function as the adhesion agents for providing stable immobilization to cell adhesion. Further verification on the long-term healing effect was obtained by evaluating the type-1 collagen expression, which plays an important role in

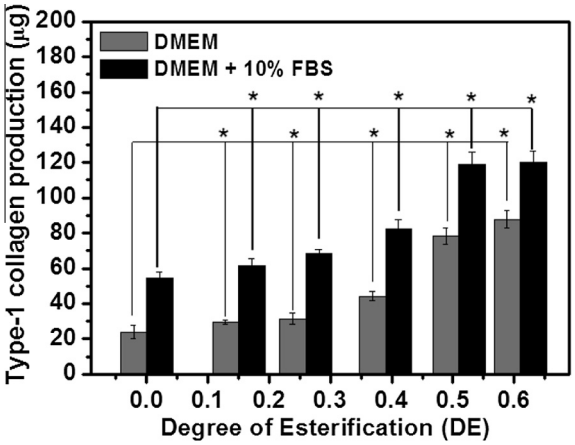

Fig. 8. The type-1 collagen production by HS68 cells cultured in the medium with (black bar) and without FBS (gray bar) after cell adhesion for 5 days. $^{*}p < 0.05$ when compared with NOCC groups (DE = 0).

tissue generation and repair [34]. After cell incubation for 5 days, the cells incubated with PMSC with the DE up to 0.51 could generate 120 μg collagen, while only 60–80 μg of collagen was produced by the cells incubated with PMSC with the DE < 0.39 (Fig. 8). This result was further verified by a test involving treatment without 10% FBS. A similar tendency was observed for the cells on the PMSC with a larger DE, consistently demonstrating that fibroblast adherence to the stiffer PMSC gels could produce more type-I collagen. This finding is well-recognized as the fibrotic tissue reactions in the healing process [35]. The results explain why the NOCC was not favorable for cell morphogenesis as shown in Fig. 4b due to inconstant environmental pH, and the excessively soft networks. However, PDMS modification could impart the resulting PMSC hybrid with optimal mechanical strength through enhancement of the network structure. Therefore, by controlling the PDMS, an optimal microenvironment for the growth of dermal cells can be suitably designed for wound healing platform via precise manipulation on the PMSC hybrids.

4. Conclusions

In summary, a new type of hierarchically structural hydrogel based on chemical hybridization of hydrophilic polysaccharide and hydrophobic polysiloxane was developed to investigate skin cell behavior. Despite the observation that poor surface wettability did not promote short-term cell attachment due to the hydrophobic character of PDMS, the self-assembling hierarchical structure of the PMSC hybrid enabled both topographical guidance and mechanical support to facilitate cell spreading and growth for long-term proliferation without any adhesive reagent. As the DE exceeded 0.39, the size of the PDMS-rich aggregates changed from nanoscale to microscale, which enhanced the tensile modulus of the NOCC up to fourfold and simultaneously enabled mechano-topographic guidance for cell adhesion. Given these results and the finding that PMSC hybrids promote type-I collagen production, the PMSC hybrids show great promise for healing applications.

Acknowledgments

This work was financially supported by the National Science Council of the Republic of China, Taiwan under Contracts NSC 102-2221-E-009-024-MY3 and by the "Aim for the Top University" program and Biomedical Electronics Translational Research Center of the National Chiao Tung University and the Ministry of Education, Taiwan, R.O.C.

Appendix A. Figures with essential color discrimination

Certain figures in this article, particularly Figs. 1–7 and Schemes 1 and 2 are difficult to interpret in black and white. The full color images can be found in the on-line version, at http://dx.doi.org/10.1016/j.actbio.2014.04.025.

Appendix B. Supplementary data

Supplementary data associated with this article can be found, in the online version, at http://dx.doi.org/10.1016/j.actbio.2014.04.025.

References

[1] Gentsch R, Borner HG. Designing three-dimensional materials at the interface to biology. In: Borner HG, Lutz JF, editors. Bioactive surfaces. Berlin: Springer; 2011. p. 163–92.
[2] Owen SC, Shoichet MS. Design of three-dimensional biomimetic scaffolds. J Biomed Mater Res A 2010;94A:1321–31.
[3] Arima Y, Iwata H. Effect of wettability and surface functional groups on protein adsorption and cell adhesion using well-defined mixed self-assembled monolayers. Biomaterials 2007;28:3074–82.
[4] Pan HA, Hung YC, Sui YP, Huang GS. Topographic control of the growth and function of cardiomyoblast H9c2 cells using nanodot arrays. Biomaterials 2012;33:20–8.
[5] Nikkhah M, Edalat F, Manoucheri S, Khademhosseini A. Engineering microscale topographies to control the cell–substrate interface. Biomaterials 2012;33:5230–46.
[6] Feng CH, Cheng YC, Chao PHG. The influence and interactions of substrate thickness, organization and dimensionality on cell morphology and migration. Acta Biomater 2013;9:5502–10.
[7] Smith BS, Yoriya S, Johnson T, Popat KC. Dermal fibroblast and epidermal keratinocyte functionality on titania nanotube arrays. Acta Biomater 2011;7:2686–96.
[8] Dhandayuthapani B, Yoshida Y, Maekawa T, Kumar DS. Polymeric scaffolds in tissue engineering application: a review. Int J Polym Sci 2011;2011:1–19.
[9] Slaughter BV, Khurshid SS, Fisher OZ, Khademhosseini A, Peppas NA. Hydrogels in regenerative medicine. Adv Mater 2009;21:3307–29.
[10] Wang YX, Robertson JL, Spillman WB, Claus RO. Effects of the chemical structure and the surface properties of polymeric biomaterials on their biocompatibility. Pharm Res 2004;21:1362–73.
[11] Anitha A, Rani VVD, Krishna R, Sreeja V, Selvamurugan N, Nair SV, et al. Synthesis, characterization, cytotoxicity and antibacterial studies of chitosan, O-carboxymethyl and N,O-carboxymethyl chitosan nanoparticles. Carbohydr Polym 2009;78:672–7.
[12] Muzzarelli RAA. Chitins and chitosans for the repair of wounded skin, nerve, cartilage and bone. Carbohydr Polym 2009;76:167–82.
[13] Berman B, Perez OA, Konda S, Kohut BE, Viera MH, Delgado S, et al. A review of the biologic effects, clinical efficacy, and safety of silicone elastomer sheeting for hypertrophic and keloid scar treatment and management. Dermatol Surg 2007;33:1291–303.
[14] Patrickios CS, Georgiou TK. Covalent amphiphilic polymer networks. Curr Opin Colloid Interface Sci 2003;8:76–85.
[15] Huang WC, Chen SY, Liu DM. An amphiphilic silicone-modified polysaccharide molecular hybrid with in situ forming of hierarchical superporous architecture upon swelling. Soft Matter 2012;8:10868–76.
[16] Chung SH, Min J. Morphological investigations of cells that adhered to the irregular patterned polydimethylsiloxane (PDMS) surface without reagents. Ultramicroscopy 2009;109:861–7.
[17] Pernodet N, Rafailovich M, Sokolov J, Xu D, Yang NL, McLeod K. Fibronectin fibrillogenesis on sulfonated polystyrene surfaces. J Biomed Mater Res A 2003;64A:684–92.
[18] Liu TY, Chen SY, Lin YL, Liu DM. Synthesis and characterization of amphiphatic carboxymethyl-hexanoyl chitosan hydrogel: water-retention ability and drug encapsulation. Langmuir 2006;22:9740–5.
[19] McDaniel DP, Shaw GA, Elliott JT, Bhadriraju K, Meuse C, Chung KH, et al. The stiffness of collagen fibrils influences vascular smooth muscle cell phenotype. Biophys J 2007;92:1759–69.
[20] Frisman I, Seliktar D, Bianco-Peled H. Nanostructuring PEG-fibrinogen hydrogels to control cellular morphogenesis. Biomaterials 2011;32:7839–46.
[21] Satriano C, Conte E, Marletta G. Surface chemical structure and cell adhesion onto ion beam modified polysiloxane. Langmuir 2001;17:2243–50.
[22] Vogler EA. Thermodynamics of short-term cell adhesion in vitro. Biophys J 1988;53:759–69.
[23] Lim JY, Shaughnessy MC, Zhou ZY, Noh H, Vogler EA, Donahue HJ. Surface energy effects on osteoblast spatial growth and mineralization. Biomaterials 2008;29:1776–84.
[24] Yang L, Li YW, Sheldon BW, Webster TJ. Altering surface energy of nanocrystalline diamond to control osteoblast responses. J Mater Chem 2012;22:205–14.

[25] Blau A. Cell adhesion promotion strategies for signal transduction enhancement in microelectrode array in vitro electrophysiology: an introductory overview and critical discussion. Curr Opin Colloid Interface Sci 2013;18:481–92.
[26] Eagle H. The effect of environmental pH on the growth of normal and malignant cells. J Cell Physiol 1973;8:8.
[27] Yin YH, Lv XL, Tu HW, Xu S, Zheng H. Preparation and swelling kinetics of pH-sensitive photocrosslinked hydrogel based on carboxymethyl chitosan. J Polym Res 2010;17:471–9.
[28] Jang J, Moon SJ, Hong SH, Kim IH. Colorimetric pH measurement of animal cell culture media. Biotechnol Lett 2010;32:1599–607.
[29] Swift J, Ivanovska IL, Buxboim A, Harada T, Dingal P, Pinter J, et al. Nuclear lamin-A scales with tissue stiffness and enhances matrix-directed differentiation. Science 2013;341:1240104–50115.
[30] Ananthakrishnan R, Ehrlicher A. The forces behind cell movement. Int J Biol Sci 2007;3:303–17.
[31] Lombardo M, Carbone G, Lombardo G, De Santo MP, Barberi R. Analysis of intraocular lens surface adhesiveness by atomic force microscopy. J Cataract Refract Surg 2009;35:1266–72.
[32] Georges PC, Janmey PA. Cell type-specific response to growth on soft materials. J Appl Physiol 2005;98:1547–53.
[33] Wozniak MA, Modzelewska K, Kwong L, Keely PJ. Focal adhesion regulation of cell behavior. Biochim Biophys Acta 2004;1692:103–19.
[34] Frazier K, Williams S, Kothapalli D, Klapper H, Grotendorst GR. Stimulation of fibroblast cell growth, matrix production, and granulation tissue formation by connective tissue growth factor. J Invest Dermatol 1996;107:404–11.
[35] Kim WS, Park BS, Sung JH, Yang JM, Park SB, Kwak SJ, et al. Wound heating effect of adipose-derived stem cells: a critical role of secretory factors on human dermal fibroblasts. J Dermatol Sci 2007;48:15–24.
[36] Yang TL. Chitin-based materials in tissue engineering: applications in soft tissue and epithelial organ. Int J Mol Sci 2011;12:1936–63.
[37] Rinaudo M. Chitin and chitosan: properties and applications. Prog Polym Sci 2006;31:603–32.
[38] Jayakumar R, Menon D, Manzoor K, Nair SV, Tamura H. Biomedical applications of chitin and chitosan based nanomaterials – a short review. Carbohydr Polym 2010;82:227–32.
[39] Jayakumar R, Prabaharan M, Kumar PTS, Nair SV, Tamura H. Biomaterials based on chitin and chitosan in wound dressing applications. Biotechnol Adv 2011;29:322–37.
[40] Yang B, Zhang YL, Zhang XY, Tao L, Li SX, Wei Y. Facilely prepared inexpensive and biocompatible self-healing hydrogel: a new injectable cell therapy carrier. Polym Chem 2012;3:3235–8.
[41] Chen YH, Chung YC, Wang IJ, Young TH. Control of cell attachment on pH-responsive chitosan surface by precise adjustment of medium pH. Biomaterials 2012;33:1336–42.
[42] Schwarz US, Balaban NQ, Riveline D, Bershadsky A, Geiger B, Safran SA. Calculation of forces at focal adhesions from elastic substrate data: the effect of localized force and the need for regularization. Biophys J 2002;83:1380–94.
[43] Montembault A, Viton C, Domard A. Rheometric study of the gelation of chitosan in aqueous solution without cross-linking agent. Biomacromolecules 2005;6:653–62.
[44] Treloar LRG. The physics of rubber elasticity. 3rd ed. Oxford: Clarendon Press; 1975.